Comparison of Choroidal Hypertransmission and Retinal Pigment Epithelium Loss for Quantification of Geographic Atrophy Across Commonly Used SD-OCT Devices

Anna Eidenberger[1,2], Klaudia Birner[1,2], Sophie Frank-Publig[1,2], Johannes Schrittwieser[1,2], Merle Tratnig-Frankl[1,2], Markus Gumpinger[2], and Ursula Schmidt-Erfurth[2]*

1 Department of Ophthalmology and Optometry, Medical University of Vienna, Vienna, Austria
2 Laboratory for Ophthalmic Image Analysis (OPTIMA), Medical University of Vienna, Vienna, Austria

Corresponding Author:

Prof. Dr. Ursula Schmidt-Erfurth

Laboratory of Ophthalmic Image Analysis (OPTIMA)

Medical University of Vienna

Spitalgasse 23, 1090 Vienna, Austria

Tel: +43 1 40400 79310

Fax: +43 1 40400 79120

Email: ursula.schmidt-erfurth@meduniwien.ac.at

Word count: 4,290 (without title page, abstract, tables, figure legends, references)

Number of Figures: 4 **Number of Tables:** 3 **Number of Supplementary Files:** 1 Table, 3 Figures

Commercial Relationships Disclosure:
AE, KB, SFB, MG, JS, MTF: none

USE: AbbVie (C), ADARx (C), Alcon (C), Alkeus (C), Allergan (C), Annexon (C), Apellis (C, F), Astellas (C), Aviceda (C), Bayer (C), Boehringer Ingelheim (C), Complement Therapeutics (C), EcoR1 (C), Galimedix (C), Genentech (F) Heidelberg Engineering (F), Janssen (C), Kodiak (C, F), Medscape (C), ONL (C), RetInSight (F), Roche (C, F), Topcon (C)

The Authors received **NO FUNDING** for this work.

Keywords: Geographic atrophy, Hypertransmission, RPE loss, Optical coherence tomography, Artificial intelligence, Deep learning

Abstract

To compare the consistency of choroidal hypertransmission (HT) and retinal pigment epithelium (RPE) loss area measurements among three commonly used spectral-domain optical coherence tomography (OCT) devices and assess their robustness for monitoring of geographic atrophy (GA). Patients with GA were imaged during a single visit using the three different OCT: (1) Heidelberg Spectralis; (2) Zeiss Cirrus; (3) Topcon Maestro2. Expert readers manually annotated a total of 120 OCT volumes for RPE loss and HT. Dice similarity coefficients (DSC) were calculated to quantify the spatial overlap between the lesions within each OCT device. Intraclass correlation coefficients (ICC) and Bland-Altman analyses were used to assess inter-device agreement. Spatial overlap between HT and RPE loss ranged from moderate to good, with HT lesions being significantly larger than RPE loss areas across all devices ($p < 0.001$). Overall agreement was good for HT and RPE loss. Systematic biases emerged, with Cirrus yielding consistently smaller measurements compared to Spectralis or Maestro2. Lesion measurements demonstrated good agreement across all three OCT devices, yet device-dependent differences require caution when comparing data. Accounting for inter-device variability is an essential step toward reliable clinical endpoints and successful integration of automated OCT algorithms into clinical trials and routine AMD care.

Introduction

As a result of irreversible deterioration of photoreceptors, the retinal pigment epithelium (RPE), and the underlying choriocapillaris, geographic atrophy (GA) secondary to age-related macular degeneration (AMD) poses a major disease burden worldwide, causing severe visual impairment [1]. Recently, the first two substances for intravitreal therapy targeting GA, pegcetacoplan and avacincaptad pegol, received regulatory approval from the Food and Drug Administration (FDA) in the United States.

The primary endpoint of the corresponding phase III studies was the change of GA lesion area measured by fundus autofluorescence imaging (FAF) [2], [3]. FAF has been the gold standard in assessing RPE integrity, as it allows for visualization of fluorophores in RPE cells and the absence of fluorophores in atrophic areas. However, spectral-domain (SD) optical coherence tomography (OCT) has emerged as the state-of-the-art diagnostic tool in the management of AMD [4], [5]. In contrast to FAF, OCT enables noninvasive visualization of the neurosensory morphology of the retina, the RPE layer, and the choroidal vasculature at a pixel level, which is critical for effectively monitoring all aspects of GA growth and detecting subtle anatomical changes [6]. Therefore, the Classification of Atrophy Meetings (CAM) group recommended OCT as the preferred imaging modality for GA detection and monitoring. They suggested defining GA in OCT as complete RPE and outer retinal atrophy (cRORA), which includes photoreceptor degeneration visible as ellipsoid zone (EZ) loss, choroidal hypertransmission (HT), and RPE loss of 250 µm or more in diameter [7]. Consequently, establishing clinical trial endpoints using OCT imaging appears inevitable.

The introduction of artificial intelligence (AI) for OCT image analysis allows for visualization and quantification of retinal layer integrity and pathology in an automated manner [8], [9]. However, the OCT technology varies by manufacturer,

creating challenges in algorithm development and validation. Consequently, biomarker consistency across commonly used OCT devices must be assessed to ensure reliable disease monitoring and interpretation of study outcomes [10]. As human annotations remain the backbone of automated AI algorithms, underlying device-specific variability requires thorough evaluation.

The CAM-based definition of cRORA provides a clinically meaningful framework for identifying GA in OCT by integrating multiple structurally relevant criteria. However, translation into reliable and quantifiable manual or automated lesion delineation may be challenging. In this study, we therefore focused on HT and RPE loss as individual and pathognomonic OCT features serving as quantitative biomarkers of GA-related structural changes [11], [12], [13]. HT and RPE loss area were quantified based on human expert annotations across three widely employed spectral-domain OCT devices (Spectralis, Maestro2, and Cirrus) to evaluate measurement consistency. Additionally, the respective manual annotations of RPE loss and HT areas were compared within the same OCT volumes to determine and validate their spatial overlap and measurement characteristics as biomarkers reflecting morphological changes of GA. This comprehensive step is essential for establishing reliable outcome parameters and advancing the use of automated tools for objective disease monitoring, both in clinical trials and, even more importantly, in clinical practice.

Methods

Study Design

A prospective single site study was performed at the outpatient retina clinic of the Medical University of Vienna based on the diagnosis of GA secondary to AMD. The diagnosis of GA was made by a retina specialist via fundus examination and based on the cRORA criteria on OCT [7]. Included GA lesions varied in size (small to large), location (foveal involvement and extrafoveal), and configuration

(unifocal and multifocal) as defined on OCT, representing a consecutive spectrum of GA patients in a routine retina service. Patients with high myopia or hyperopia (> +6.0 diopters, < -6.0 diopters) were not eligible. Patients were excluded if signs of macular neovascularization were present in OCT-angiography or visible by subretinal fluid or intraretinal fluid on OCT. Additional exclusion criteria included ocular comorbidities, such as any form of glaucoma with a cup-to-disc ratio greater than 0.8 or intraocular pressure exceeding 25 mmHg. Eyes with cataract, posterior capsular opacification, or other relevant refractive anomalies were excluded based on characteristic deterioration in OCT image quality, such as reduced signal strength, increased speckle noise, or shadowing artifacts. Sufficient image quality was assessed according to previously established criteria for quantitative retinal layer analysis. OCT volumes were excluded if one of the following conditions was present in one or more B-scans [14]: (1) mirroring of retinal bands, (2) capping of the retinal bands, (3) blurred images precluding reliable segmentation, and (4) decentered scans, in which the fovea was located outside the central 1-mm OCT region. If both eyes met the inclusion criteria, the eye with superior image quality was selected. Image quality was assessed based on signal-to-noise ratio, background noise, clarity of the GA lesion borders and the presence of motion artifacts on the en face image. In the case of comparable image quality, the eye with the larger GA area was selected.

The protocol received approval from the Ethics Committee of the Medical University of Vienna (EC: 2094/2018) and study procedures followed the tenets of the Declaration of Helsinki. All patients gave written informed consent prior to enrollment.

Imaging protocol

Prior to OCT acquisition, one drop of 0.5% tropicamide was administered to the imaged eye for pupil dilation. Patients were imaged with three different SD-OCT

devices during one single-day visit. The OCT scans covered the volume of 6 mm x 6 mm x 2 mm of the macula and were acquired with a Cirrus 5000 HD-OCT (Carl Zeiss Meditec, Inc., Dublin, CA, United States) including 128 B-scans by 512 x 1024 pixels, Heidelberg Spectralis HRA + OCT (Heidelberg Engineering, Heidelberg, Germany) including 49 or 97 B-scans by 1024 x 496 pixels, and Topcon 3D OCT-Maestro2 (Topcon, Tokyo, Japan) including 128 B-scans by 512 x 885 pixels. In Spectralis both raster densities (49 and 97 B-scans) correspond to standard clinical protocols and were used to reflect routine imaging practice within this prospective study, mirroring the real-world setting from the outpatient clinic. In patients with advanced GA and reduced fixation stability, a less dense protocol with a lower acquisition time was preferred to ensure adequate image quality and reduce motion artifacts [15]. The technical properties of each device are listed in Table 1.

Table 1. Technical Properties of each OCT device (adapted from [10])

Device	**Wavelength**	**Scanning Speed (A-scan/s)**	**Axial resolution***
SD-OCT Zeiss Cirrus 5000 HD-OCT	840 nm	27,000/s	5 µm
SD-OCT Heidelberg Spectralis HRA + OCT	870 nm	85,000/s	7 µm
SD-OCT Topcon 3D OCT-1 Maestro2	840 nm	50,000/s	6 µm

*The axial resolution value refers to the tissue-equivalent resolution.

SD = spectral-domain; OCT = optical coherence tomography

Segmentation procedures

Retinal layers were initially automatically segmented using the Iowa Reference Algorithm. The Iowa Reference Algorithm is a widely validated graph-theoretical method applied to volumetric data from various SD-OCT devices, developed by the Retinal Image Analysis Lab (Iowa Institute for Biomedical Imaging, Iowa City,

Iowa) [16]. To determine the areas of RPE loss, the automated segmentation was then followed by manual adjustments to the inner border of the RPE layer (Figure 2). In the presence of a disrupted RPE the segmentation line was terminated at the end of the hyperreflective RPE bands visible on each B-Scan. Segmentation of HT area was entirely based on manual annotations, which were performed on an A-scan basis per B-scan (Figure 2). HT was defined as an area of increased light transmission in the choroid, appearing at least twice as bright as the reflectance of the surrounding choroid, irrespective of the overlying retinal structure. RPE loss and HT lesions had no minimum size requirements. Examples of manual annotations for each OCT device are provided in the Supplementary Figures S1-S3.

All manual corrections were performed by trained readers, which were validated by expert readers trained according to reading center standards in a second run (SFP, KB, AE) to allow for human expert-based comparison of the devices. All readers had access to a standardized reading manual aligned with the consensus definition of GA during the entire reading process. Meetings for supervision were held weekly by the expert readers to review ambiguous cases with the trained readers. Challenging cases were discussed among the expert readers until consensus was achieved. Annotations were performed independently for each device, with readers masked to segmentations from the other devices. For Spectralis OCT images corrections were performed in 49 B-Scans per volume, and for Cirrus and Maestro2 OCT images, every second B-scan was annotated, manually correcting 64 B-scans per volume. RPE loss and HT area were computed in mm^2 as 2D-en face maps reflecting the lesions of discontinued RPE and the A-scan regions of HT within the 6-mm Early Treatment Diabetic Retinopathy Study (ETDRS)-grid. To ensure consistency across the analyzed ETDRS-region across each OCT device, the foveal center was manually aligned in all OCT volumes. En face pixel spacing was derived individually for each scan from device-specific

DICOM metadata. Lesion areas were calculated in mm^2 by multiplying the number of lesion-positive pixels by the corresponding lateral pixel area. This device- and scan-specific scaling ensured accurate physical area quantification without assuming uniform pixel dimensions across OCT devices.

Statistical analysis

Data distribution was evaluated using histograms for visualization. For non-parametric distributions, results were presented as median and interquartile range (IQR). The Friedman test was performed to assess significant differences in lesion size across the three OCT devices, with pairwise post hoc comparisons. Bonferroni method was applied to correct p-values for multiple testing. As each patient was imaged using all three OCT devices, intraclass correlation coefficients (ICC) were calculated using a two-way mixed-effects model (ICC [3,1]), to determine the absolute agreement of RPE loss and HT area measurements across the devices. Additionally, the Dice similarity coefficient (DSC) was calculated for each OCT volume to determine the spatial overlap between RPE loss and HT regions. ICC and DSC values were interpreted as follows: A value below 0.50 was considered poor; a value between 0.50 and 0.75 was considered moderate; a value between 0.75 and 0.90 was considered good; and a value above 0.90 was considered excellent.

For direct comparisons between the OCT devices, Bland-Altmann plots were created for each pair of devices (Spectralis, Maestro2, Cirrus), showing the mean of the two device lesion measurements (x-axis) against their difference (y-axis). The Bland-Altman plots provide an assessment of bias (mean difference) and variability (limits of agreement [LoA]) in area measurements. Statistical analyses and plots were performed in R (version 4.4.3) using custom scripts based on ggplot2. All statistical tests were two-sided, and a p-value < 0.05 was considered statistically significant.

Results

A total of 120 OCT volumes from 40 eyes of 40 patients from each of the three OCT devices were included in this prospective study, yielding area measurements of 7,080 OCT B-scans. The mean age of patients was 79.9 ± 6.8 years and 31 (77.5%) were female. Among the 40 eyes analyzed, 28 (70.0%) exhibited GA lesions smaller than the 0.5 disc area (defined as 1.33 mm^2), 13 (32.5%) presented with a unifocal configuration, and 26 (65.0%) demonstrated foveal involvement.

Quantitative differences in RPE loss and hypertransmission in the different devices

Descriptive statistics for RPE loss and HT area measurements are presented in Table 2. In the Friedman test a statistically significant difference in RPE loss area measurements among the three OCT devices ($p < 0.001$) was found. Pairwise comparison of RPE loss area revealed significantly larger measurements in Spectralis and Maestro2 OCT volumes compared to the Cirrus OCT, with p-values of 0.004 and 0.036, respectively. In contrast, no significant difference between Spectralis and Maestro2 was found ($p = 0.127$). We observed a similar pattern for HT area measurements. The Friedman test indicated a highly significant difference among the three devices ($p < 0.001$). Median lesion areas were greater in Spectralis and Maestro2 compared to Cirrus, both with p-values < 0.001. However, the difference between Spectralis and Maestro2 was not statistically significant ($p = 1.000$).

Table 2. Descriptive Statistics, Intraclass Correlation Coefficient and Dice similarity coefficient on Area of Hypertransmission and RPE loss across the three OCT devices

	Median (IQR)	ICC [Spectralis - Maestro – Cirrus]

	Spectralis		Maestro2		Cirrus			
Hypertransmission area [mm²]	1.11	(0.85 to 2.31)	1.18	(0.69 to 1.98)	0.76	(0.53 to 1.72)	0.83	(95% CI 0.74 to 0.90)
RPE loss area [mm²]	0.77	(0.47 to 1.63)	0.61	(0.44 to 1.43)	0.54	(0.31 to 1.18)	0.80	(95% CI 0.69 to 0.88)
DSC (HT-RPE-area Overlap)	0.76	(0.64 to 0.85)	0.72	0.60 to 0.80)	0.73	(0.60 to 0.81)		

CI = Confidence Interval; Cirrus = Cirrus 5000 HD-OCT (Carl Zeiss Meditec, Inc.), DSC = Dice similarity coefficient, HT = Hypertransmission, ICC = intraclass correlation coefficient, Maestro2 = Topcon 3D OCT Maestro2 (Topcon), RPE = retinal pigment epithelium, Spectralis = Spectralis HRA + OCT (Heidelberg Engineering).

The ICC demonstrated good agreement among the three OCT devices for both RPE loss (ICC = 0.80) and HT area measurements (ICC = 0.82). Supplementary Table S1 provides an overview of the pairwise agreement comparisons. The DSC ranged from 0.72 to 0.76, reflecting moderate to good spatial overlap between HT regions and RPE loss lesions within each device (Figure 1). Notably, HT areas were consistently larger than the RPE loss areas within the 6-mm ETDRS-grid across all OCT devices (Table 2; all $p < 0.001$).

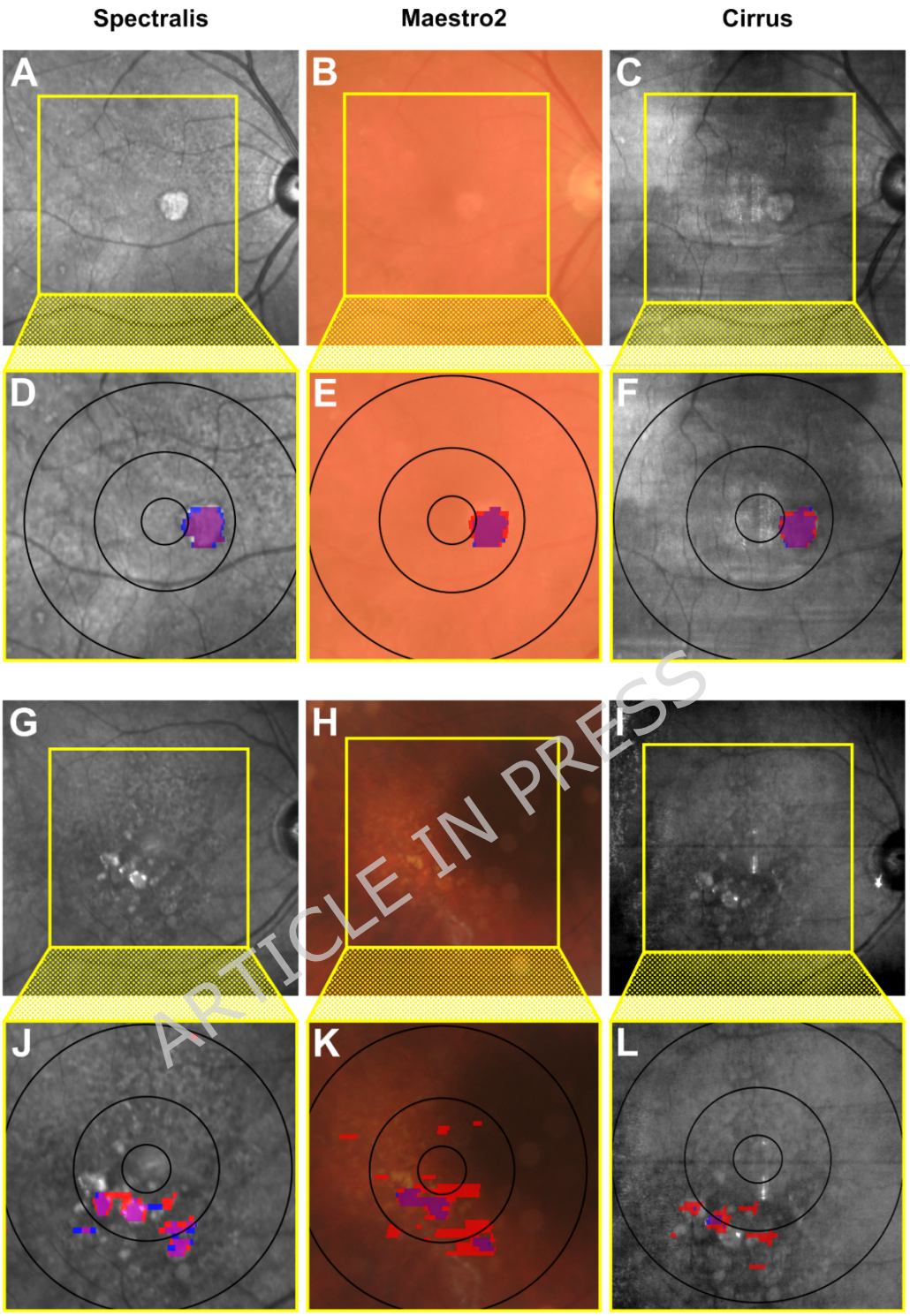

Figure 1. *Examples of spatial overlap between manually annotated hypertransmission and RPE loss within each device for an eye with a unifocal GA lesion showing good spatial overlap* ***(A-F)*** *and for an eye with a multifocal GA lesion demonstrating fair spatial overlap* ***(G-L)****. En face projections are derived from manual OCT B-scan annotations and overlaid on the corresponding nIR acquired simultaneously with the OCT in Spectralis and Cirrus, and overlaid on the corresponding CFP acquired simultaneously with the OCT in*

Maestro2. ***D-F)*** *demonstrate a good spatial overlap (purple) between projected 2-D area of hypertransmission (red) based on the A-scan per B-Scan annotations and RPE loss (blue) based on the pixel-wise layer annotations.* ***J-L)*** *demonstrate a fair spatial overlap (purple) between projected 2-D area of hypertransmission (red) based on the A-scan per B-Scan annotations of RPE loss based on the pixel-wise layer annotations. CFP = color fundus photography, Cirrus = Cirrus 5000 HD-OCT (Carl Zeiss Meditec, Inc.), Maestro2 = Topcon 3D OCT Maestro2 (Topcon), nIR = near infrared reflectance, RPE = retinal pigment epithelium, Spectralis = Spectralis HRA + OCT (Heidelberg Engineering).*

Qualitative differences between devices

Figure 2 displays representative B-scan examples obtained from the three OCT devices, comparing qualitative differences between the acquired OCT volumes. The B-scans show variability across the devices, with Spectralis offering the highest signal-to-noise ratio characterized by minimal speckle noise. This results in a more-defined separation of the retinal layers and visualization of morphological details because of its broader reflectivity range and higher contrast. In comparison, images obtained from the Maestro2 and Cirrus devices exhibit lower contrast and higher levels of background noise. Nonetheless, key structural features, including the outer retinal bands, remain well delineated in all devices.

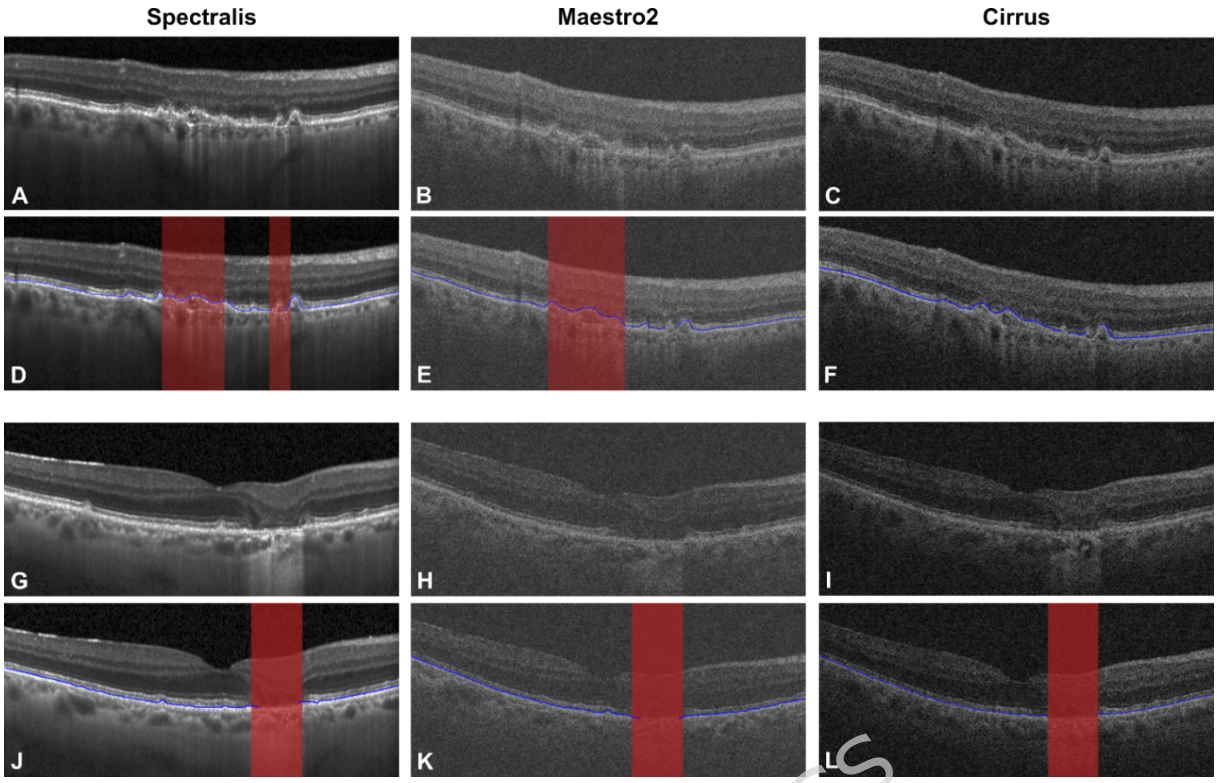

Figure 2. Representative OCT B-scans acquired using the three OCT devices (Spectralis, Maestro2, and Cirrus) displaying qualitative differences in image quality. The Spectralis B-scans (left column) show enhanced layer contrast, reduced speckle noise, and improved delineation of retinal structure. In comparison, the Maestro2 (middle column) and Cirrus (right column) B-scans exhibit lower contrast and increased speckle noise levels

Table 3. Mean Difference, Standard Deviation of Difference, Upper and Lower Limits of Agreement from the Bland-Altmann-Plots across all Pairwise OCT device Comparisons

Device Comparison	Hypertransmission area [mm^2]	RPE loss area [mm^2]
	Mean Difference	**Mean Difference**
Cirrus - Spectralis	-0.43	-0.25
Maestro2 - Spectralis	-0.05	-0.11
Cirrus - Maestro2	-0.39	-0.14

	Standard Deviation of Difference	**Standard Deviation of Difference**
Cirrus - Spectralis	± 1.03	± 0.81
Maestro2 - Spectralis	± 0.31	± 0.36

Cirrus - Maestro2	± 1.00		± 0.76	

	Upper LoA	Lower LoA	Upper LoA	Lower LoA
Cirrus - Spectralis	1.58	-2.44	1.34	-1.84
Maestro2 - Spectralis	0.57	-0.66	0.6	-0.82
Cirrus - Maestro2	1.59	-2.36	1.34	-1.62

CI = confidence interval, Cirrus = Cirrus 5000 HD-OCT (Carl Zeiss Meditec, Inc.), HT = Hypertransmission, LoA = Limits of Agreement, Maestro2 = Topcon 3D OCT Maestro2 (Topcon), RPE = retinal pigment epithelium, Spectralis = Spectralis HRA + OCT (Heidelberg Engineering).

Agreement Analyses

The results from the agreement analyses for each OCT pair of HT and RPE loss area in the 6-mm ETDRS-grid are summarized in Table 3. Bland-Altman plots displayed variable degrees of agreement in both HT and RPE loss area measurements across the three OCT devices (Figure 3). The pairwise comparison of Cirrus and Spectralis showed the largest discrepancy for HT area, with a mean difference of -0.43 mm^2 ± 1.03 with high variability (LoA -2.44 to 1.58 mm^2; Table 3). The Cirrus-Maestro2 pair similarly showed a mean difference of -0.39 mm^2 ± 1.00 (LoA -2.36 to 1.59 mm^2), reflecting consistent overestimation of HT area on Maestro2 in relation to Cirrus. The Spectralis-Maestro2 comparison demonstrated excellent agreement, with minimal bias (-0.05 mm^2 ± 0.31) and narrow LoA (-0.66 to 0.57 mm^2; Table 3).

Bland-Altman plots comparing RPE loss area across device pairs revealed similar, but more consistent trends. Measurements on Cirrus tended to underestimate RPE loss area relative to measurements on Spectralis and Maestro2, with mean differences of -0.25 mm^2 ± 0.81 (LoA -1.84 to 1.34 mm^2) and -0.14 mm^2 ± 0.76 (LoA -1.62 to 1.34 mm^2), respectively. The best agreement for RPE loss area was observed between Spectralis and Maestro2, with a small mean difference of -0.11

mm^2 ± 0.36 and the lowest variability (LoA -0.82 to 0.60 mm^2). Importantly, a trend of increasing variability in RPE loss and HT area measurement differences with larger lesion sizes is displayed across all Bland-Altman plots. This heteroscedastic pattern indicates a decrease in inter-device agreement as lesion size increases, whereas smaller lesions exhibit more consistent measurements.

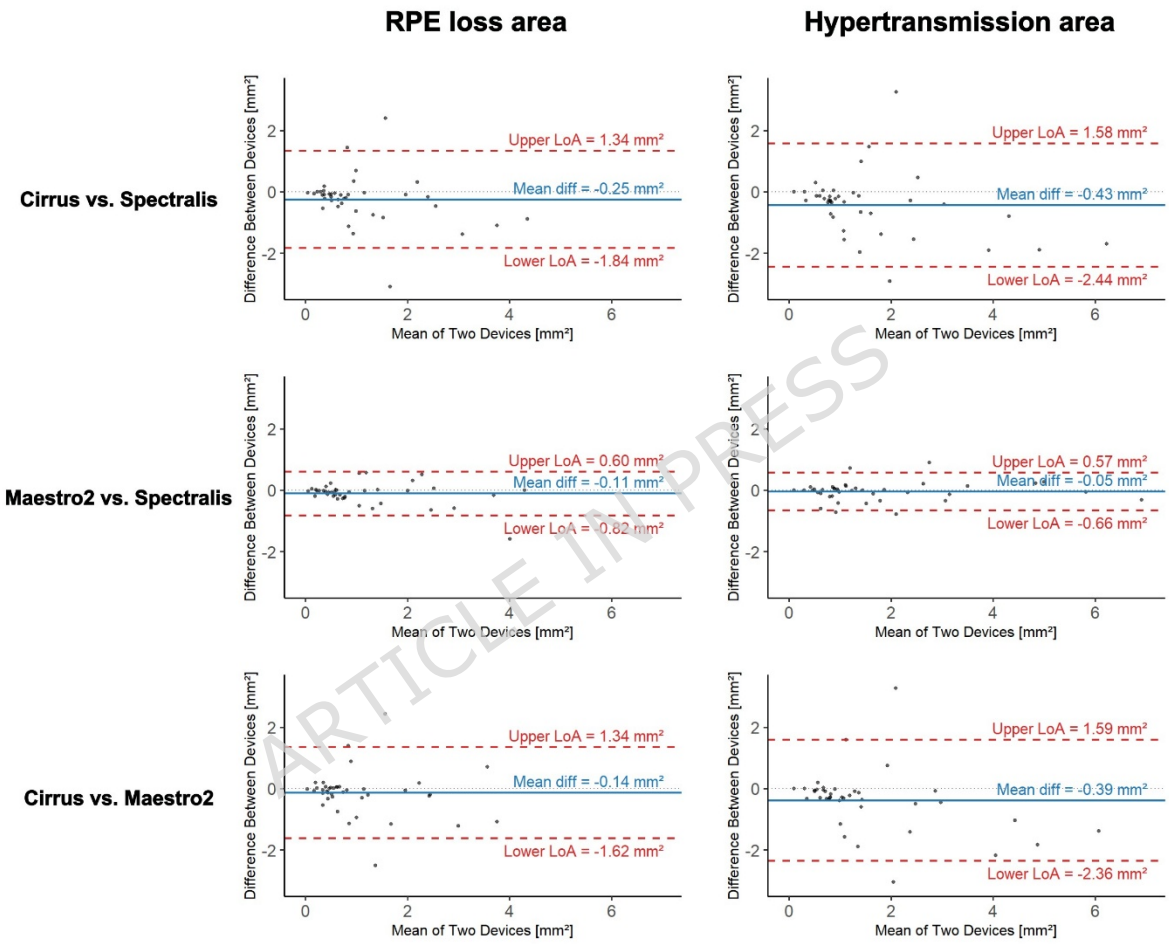

Figure 3*. Bland-Altman plots illustrating the bias and variability of RPE loss and HT area measurements in mm^2 across Spectralis, Maestro2 and Cirrus OCT devices. The 95% Limits of Agreement (Mean Difference ±1.96 Standard Deviation of the Difference) are plotted with red. The blue line indicates the Mean Difference between the measurements in mm^2. Cirrus = Cirrus 5000 HD-OCT (Carl Zeiss Meditec, Inc.), HT = hypertransmission, Maestro2 = Topcon 3D OCT Maestro2 (Topcon), RPE = retinal pigment epithelium, Spectralis = Spectralis HRA + OCT (Heidelberg Engineering).*

To account for this scale-dependent variability, square-root transformation was applied to lesion area measurements and reassessed in Bland-Altman analysis (Figure 4). Heteroscedasticity was reduced by the transformation and resulted in a more uniform distribution of measurement differences across the lesion size spectrum. The transformation confirmed, that variability in raw measurements was largely driven by lesion size rather than systematic device bias.

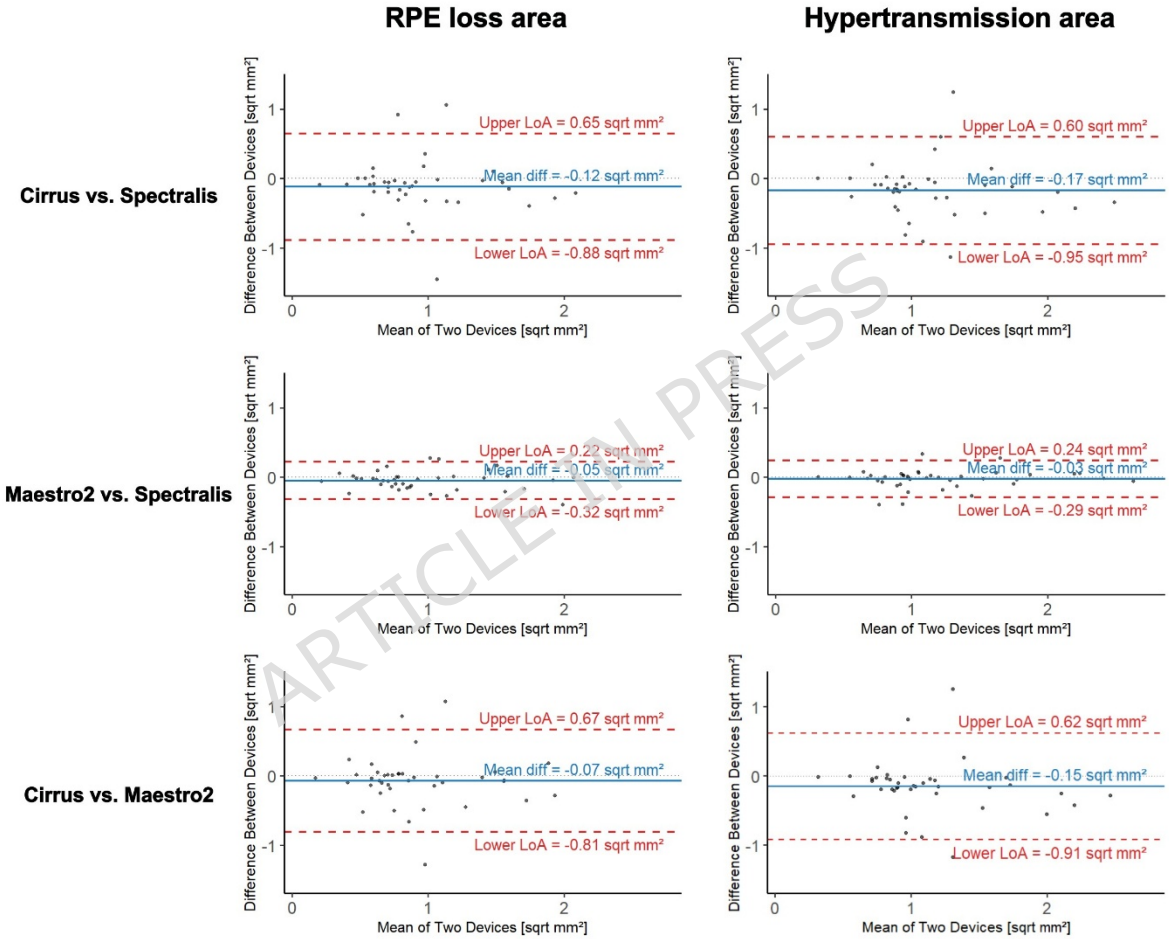

Figure 4. *Bland-Altman plots illustrating the bias and variability of RPE loss and HT area measurements in √mm² across Spectralis, Maestro2 and Cirrus OCT devices. The 95% Limits of Agreement (Mean Difference ±1.96 Standard Deviation of the Difference) are plotted with red. The blue line indicates the Mean Difference between the measurements in √mm². Cirrus = Cirrus 5000 HD-OCT (Carl Zeiss Meditec, Inc.), HT =*

hypertransmission, Maestro2 = Topcon 3D OCT Maestro2 (Topcon), RPE = retinal pigment epithelium, Spectralis = Spectralis HRA + OCT (Heidelberg Engineering).

Discussion

In this prospective comparison study, we evaluated the accuracy and reproducibility of RPE loss and HT area measurements in three commonly used SD-OCT devices to establish their robustness for detecting and quantifying atrophic lesions secondary to GA. In general, we found good inter-device agreement for both RPE loss and HT area measurements indicating consistency in quantifying lesion size. Both RPE-loss and HT area measurements were consistently smaller on Cirrus compared to Spectralis and Maestro2. Bland-Altman analyses demonstrated a systematic underestimation of area measurements in Cirrus, with greater variability in pairwise comparisons involving Cirrus and either Spectralis or Maestro. In contrast, no significant differences were observed between Spectralis and Maestro2 for either RPE-loss area or HT lesion size, and the mean differences and variability remained minimal when comparing these two devices. Understanding the technical specifications of the OCT devices and their impact on lesion quantification is crucial to understand differences in measurement outcomes.

Spectralis is equipped with confocal scanning laser ophthalmoscopy technology and advanced eye tracking, allowing for repeated scans at the same anatomical location over time. It uses longer center wavelengths (870 nm), enabling enhanced penetration into deeper retinal layers (e.g., RPE layer), but it has a slightly lower axial resolution – essential for distinguishing between two points along the z-axis – compared to Cirrus and Maestro2. Despite this disadvantage, the Spectralis' acquisition speed of 85,000 A-scans per second and averaging capabilities substantially enhance the signal-to-noise ratio, reduce motion artifacts, and improve image contrast [10], [17]. As a result, Spectralis offers the

sharpest layer delineation, which is useful for identifying microstructural changes (e.g., RPE loss) and provides high contrast, which is beneficial for detecting HT. In contrast, the Maestro2 OCT uses a shorter wavelength (840nm), potentially improving choroidal contrast, as light transmission predominantly occurs in regions with discontinued RPE, thereby facilitating HT quantification against the darker choroidal background [18]. Although Spectralis offers superior overall layer delineation, Maestro2 also demonstrates good reliability in delineating RPE loss, with minimal bias, likely due to its relatively high acquisition speed of 50,000 A-scans per second [10]. Given that the wavelengths of Cirrus and Maestro2 are similar, comparable image quality might be expected; however, the two devices differ notably in scanning speed. Cirrus operates at 27,000 A-scans per second, about half the speed of the Maestro2 OCT [10]. This prolonged scanning time of Cirrus might lead to increased motion artifacts distorting the OCT image, as a result reducing contrast and consequently the likelihood of accurately detecting HT. Conversely, the longer acquisition time allows more light to be captured, which potentially enhances the signal-to-noise ratio and thereby improves overall signal quality. Because the slower acquisition also results in fewer A-scans over time, the sampling density is reduced, thereby diminishing the beneficial effect of higher axial resolution. In consequence, the level of detail is reduced, making subtle anatomical changes, such as RPE loss, more difficult to discern [17]. In summary, Spectralis offers the clearest delineation of retinal layers and image contrast as a result of its high acquisition speed, combined with compensatory averaging capability, and deeper tissue penetration, making it optimal for monitoring subtle microstructural retinal changes and HT. Maestro2 also reliably depicts RPE loss and HT due to its shorter wavelength and high acquisition speed, whereas Cirrus may, in some cases, exhibit reduced image quality owing to slower scanning speed and increased motion artifacts. In the present study we focused on SD-OCT devices, since they are used as state-of-the art in clinical practice and

clinical trials assessing GA lesion growth most commonly rely on SD-OCT imaging [2], [3]. However, there is increasing literature on application of swept-source (SS)-OCT for the quantification of HT [19], [20]. SS-OCT operates at longer center wavelengths, offers faster acquisition speed, and enables deeper tissue penetration, making it favorable for choroidal visualization. However, this typically comes at the expense of axial resolution, which may influence the depiction of subtle anatomical changes of the retina such as RPE loss [21]. Therefore, our results should not be directly extrapolated to SS-OCT and device-specific validation remains essential.

In each device, the HT region measurements were significantly larger compared to the RPE loss area. Analyzing the spatial overlap of HT and RPE loss for lesions within each OCT volume revealed moderate to good correspondence. The CAM Report 6, which assessed the interreader agreement in Spectralis OCT for OCT features associated with GA progression, suggest choroidal HT as the most robust and reproducible feature, showing the highest agreement among readers when defining its extension. In contrast, a high variability evaluating RPE disruption or attenuation was described [22], [23]. However, automated delineation of the GA area based on HT region segmentation reached only moderate correlation with manual FAF-based GA area measurements [24]. Notably, the agreement improved after manual correction for segmentation errors. These segmentation errors were attributed to reduced signal strength or the presence of residual basal laminar deposits (BLamD) or debris in the atrophic region, which reduce the contrast between HT and background choroid. This highlights a potential limitation of using HT as a standalone surrogate for GA area: light transmission is often blocked in areas of RPE loss as structural remnants such as BLamD, debris, hyperreflective foci, calcified drusen, or overlying vessels are present [24]. Conversely, enhanced light transmission can occur in areas with attenuated RPE and overlying photoreceptor degeneration, even in the absence of visible RPE loss

which is also demonstrated in our study by the discrepancy in lesion size together with moderate to good spatial overlap, suggesting that HT regions were also located outside of definite RPE loss [25]. In contrast, Mai et al. demonstrated that automated GA quantification based on complete loss of the RPE layer in OCT showed a strong correlation with manual GA measurements on FAF, supporting the suitability of RPE loss as a reliable and quantifiable OCT biomarker for GA [26].

While OCT technology provide detailed information on structural changes of the retinal layers in GA, functional outcome parameters are essential to capture the clinical relevance and to assess evidence of therapeutic efficacy. Despite being the primary endpoint in GA trials until now, a clinically relevant superiority in BCVA outcomes has not been demonstrated in any phase 3 GA study [27]. Recently, microperimetry (MP) has emerged as a widely studied tool for objective functional assessment in GA, as it captures topographic changes in function [28]. A recent point-to-point analysis co-registering structural biomarkers identified via OCT with functional assessments from mesopic microperimetry showed a localized reduction in retinal sensitivity ranging from -9 to -11 decibels in regions exhibiting retinal RPE loss [29]. Given that HT on SD-OCT represents a physical light transmission phenomenon rather than a definitive morphological correlate, whereas RPE loss indicates a true biological structural change, integration of RPE-based OCT biomarkers with functional measures may offer a more reliable framework for objective GA monitoring. In recent days, AI-based tools automatically quantifying structural RPE loss have undergone extensive validation and have been shown to perform at the levels of human experts' interreader agreement [13], [27], [30]. Together, these advances in automated quantification of robust biomarkers and objective structure-function testing lay the foundation for reliable outcome measures, to allow for improved assessment of therapeutic success and personalized monitoring strategies in GA

management. However, our systematic comparison of the key features in different devices clearly demonstrate an indispensable need to validate each automated tool separately for individual devices. Obviously, the photoreceptor condition represented by the EZ layer is another relevant anatomical and functional feature in GA lesions. Advanced analyses have demonstrated that EZ loss precedes RPE loss with RPE expanding consecutively into preexisting EZ loss [30]. Moreover, the EZ/RPE loss ratio is a prognostic value for lesion progression as well as therapeutic benefit [27]. Such structural correlations represent most important guidance for GA management and are not transferable to the physical phenomena represented by HT.

Limitations of this study need to be acknowledged. First, the small sample size amplifies the impact of outliers, distorting the mean difference and reducing the stability and generalizability of the LoA from the Bland-Altman analysis. However, excluding these outliers would not accurately reflect real-world, as they are representative of variability encountered in clinical practice. Strengths of our study are the use of identical lesion imaging and identical manual reading protocols. Second, a different number of B-scans across devices was annotated (49 in Spectralis vs. 64 in Maestro2 and Cirrus), which may limit the direct comparability of measurements between devices. Although previous studies have shown no significant differences in fluid volume quantification between 128 and 64 B-scans, suggesting that 49 and 64 B-scans may yield comparable area measurements; however, this assumption requires validation [31]. Specifically, future studies are needed to determine the minimum number of B-scans required for reliably quantifying of RPE loss and HT area. Third, axial eye length measurements were not performed and therefore could not be included in the area calculations, which may have introduced scaling-related variability between devices, since lateral magnification depends on ocular biometry [32]. However, lateral pixel spacing was derived from OCT-specific metadata and inter-device

comparisons were performed within the same eye, which means at a constant axial eye length. In addition, primary exclusion of eyes with high myopia or hyperopia minimized the impact of scaling-related effects. Nevertheless, in future studies the incorporation of axial biometry may further improve inter-device standardization. Further, it must be acknowledged that due to the substantial time required for manual pixel-wise annotation of OCT volumes, taking up to seven hours per volume comprising 49-64 B-scans, no formal inter- or intra-reader agreement was conducted. However, to ensure annotation consistency, regular supervision meetings were held, and ambiguous cases were reviewed and discussed among expert readers until consensus was reached. Importantly, prior studies have extensively evaluated inter- and intrareader agreement for RPE loss and HT, demonstrating moderate to substantial agreement [13], [22], [23], [33], and thereby providing a well-established framework for the reliability of expert-based annotations of both RPE loss and HT.

While the cRORA criteria provide a standardized terminology for defining GA in OCT, they primarily summarize qualitative features, rather than quantitative measures, which are, however, most relevant for precise disease progression monitoring. Therefore, the implementation for manual and especially automated longitudinal lesion quantification is challenging, as each feature may differ in its depiction across OCT devices and a simultaneous reliable visualization of all defining criteria is highly dependent on image quality. For disease monitoring, meaningful study outcome measures and also algorithm development, there is a need for reliable OCT biomarker definitions that can be delineated consistently and are validated across devices.

This study systematically compared RPE loss and HT area in patients with GA across three commonly used SD-OCT devices. These findings reinforce RPE loss as a robust and biologically specific biomarker for GA, showing overall narrower LoA across device comparisons, indicative of lower inter-device variability, and

supported by prior findings demonstrating clinically meaningful structure/function correlations. In contrast, HT reflects a light-transmission phenomenon whose extent may be influenced by additional structural and signal-related factors beyond retinal layer atrophy. The fragmentation of HT as a signal is also highlighted by its labelling as a “barcode” feature. In conclusion, although both RPE loss and HT can be quantified reliably across devices, switching OCT systems may lead to variability in GA area measurements and should considered in clinical and research settings, underscoring the importance of device selection and imaging protocols when monitoring GA lesion progression.

Acknowledgements

The authors used ChatGPT (OpenAI, version: GPT-4o, accessed April 2025) to improve the grammar and style in this manuscript. All content edited using ChatGPT was reviewed and verified for accuracy by the authors.

Data availability

Data that support the findings of this study are available upon reasonable request from the corresponding author

Author contributions

AE, KB, SFP, USE: conception and design of the study. AE, KB, SFP, JS, MTF, MG: data collection and analysis. AE, USE: interpretation of the data. AE: preparation of manuscript. All authors were responsible for critical revision of the manuscript and final approval of the manuscript.

References

[1] J. S. Sunness *et al.*, “Enlargement of atrophy and visual acuity loss in the geographic atrophy form of age-related macular degeneration,” *Ophthalmology*, vol. 106, no. 9, pp. 1768–1779, Sep. 1999, doi: 10.1016/S0161-6420(99)90340-8.

[2] J. S. Heier *et al.*, “Pegcetacoplan for the treatment of geographic atrophy secondary to age-related macular degeneration (OAKS and DERBY): two multicentre, randomised, double-masked, sham-controlled, phase 3 trials,” *The Lancet*, vol. 402, no. 10411, pp. 1434–1448, Oct. 2023, doi: 10.1016/S0140-6736(23)01520-9.

[3] A. M. Khanani *et al.*, “Efficacy and safety of avacincaptad pegol in patients with geographic atrophy (GATHER2): 12-month results from a randomised, double-masked, phase 3 trial,” *The Lancet*, vol. 402, no. 10411, pp. 1449–1458, Oct. 2023, doi: 10.1016/S0140-6736(23)01583-0.

[4] A. P. Göbel, M. Fleckenstein, S. Schmitz-Valckenberg, C. K. Brinkmann, and F. G. Holz, “Imaging geographic atrophy in age-related macular degeneration,” Oct. 2011. doi: 10.1159/000330420.

[5] U. Schmidt-Erfurth, S. Klimscha, S. M. Waldstein, and H. Bogunović, “A view of the current and future role of optical coherence tomography in the management of age-related macular degeneration,” Jan. 01, 2017, *Nature Publishing Group*. doi: 10.1038/eye.2016.227.

[6] B. U. Pandya, M. Grinton, E. D. Mandelcorn, and T. Felfeli, “Retinal Optical Coherence Tomography Imaging Biomarkers: A Review of the Literature,” *Retina*, Dec. 2023, doi: 10.1097/IAE.0000000000003974.

[7] R. H. Guymer *et al.*, “Incomplete Retinal Pigment Epithelial and Outer Retinal Atrophy in Age-Related Macular Degeneration: Classification of Atrophy Meeting Report 4,” in *Ophthalmology*, Elsevier Inc., Mar. 2020, pp. 394–409. doi: 10.1016/j.ophtha.2019.09.035.

[8] M. L. Enzendorfer, M. Tratnig-Frankl, A. Eidenberger, J. Schrittwieser, L. Kuchernig, and U. Schmidt-Erfurth, “Rethinking Clinical Trials in Age-Related Macular Degeneration: How AI-Based OCT Analysis Can Support Successful Outcomes,” *Pharmaceuticals*, vol. 18, no. 3, p. 284, Feb. 2025, doi: 10.3390/ph18030284.

[9] G. S. Reiter *et al.*, “AI in the clinical management of GA: A novel therapeutic universe requires novel tools,” *Prog Retin Eye Res*, vol. 103, p. 101305, Nov. 2024, doi: 10.1016/j.preteyeres.2024.101305.

[10] K. Kostolna *et al.*, “A Systematic Prospective Comparison of Fluid Volume Evaluation across OCT Devices Used in Clinical Practice,” *Ophthalmology Science*, vol. 4, no. 3, p. 100456, May 2024, doi: 10.1016/j.xops.2023.100456.

[11] M. Pfau *et al.*, “Progression of Photoreceptor Degeneration in Geographic Atrophy Secondary to Age-related Macular Degeneration,” *JAMA Ophthalmol*, vol. 138, no. 10, pp. 1026–1034, Oct. 2020, doi: 10.1001/jamaophthalmol.2020.2914.

[12] S. C. Cleland *et al.*, “Quantification of Geographic Atrophy Using Spectral Domain OCT in Age-Related Macular Degeneration,” *Ophthalmol Retina*, vol. 5, no. 1, pp. 41–48, Jan. 2021, doi: 10.1016/j.oret.2020.07.006.

[13] J. Mai *et al.*, “Clinical validation for automated geographic atrophy monitoring on OCT under complement inhibitory treatment,” *Sci Rep*, vol. 13, no. 1, Dec. 2023, doi: 10.1038/s41598-023-34139-2.

[14] S. Frank-Publig *et al.*, “Quantifications of Outer Retinal Bands in Geographic Atrophy by Comparing Superior Axial Resolution and Conventional OCT,” *Invest Ophthalmol Vis Sci*, vol. 66, no. 4, p. 65, Apr. 2025, doi: 10.1167/iovs.66.4.65.

[15] M. S. Morsy *et al.*, “Comparison of Ultra-high speed 250 kHz OCTA With High speed 125 kHz Mode Using Heidelberg Spectralis SHIFT: A Paired-Eye Analysis.,” *Retina*, Dec. 2025, doi: 10.1097/IAE.0000000000004751.

[16] M. D. Abràmoff, M. K. Garvin, and M. Sonka, “Retinal imaging and image analysis.,” *IEEE Rev Biomed Eng*, vol. 3, pp. 169–208, 2010, doi: 10.1109/RBME.2010.2084567.

[17] S. Marschall, B. Sander, M. Mogensen, T. M. Jørgensen, and P. E. Andersen, “Optical coherence tomography—current technology and applications in clinical and biomedical research,” *Anal Bioanal Chem*, vol. 400, no. 9, pp. 2699–2720, Jul. 2011, doi: 10.1007/s00216-011-5008-1.

[18] A. Mahmoudi *et al.*, “Atrophic Lesions Associated with Age-Related Macular Degeneration,” *Ophthalmol Retina*, vol. 8, no. 4, pp. 367–375, Apr. 2024, doi: 10.1016/j.oret.2023.10.011.

[19] R. Laiginhas *et al.*, “Persistent Hypertransmission Defects Detected on En Face Swept Source Optical Computed Tomography Images Predict the Formation of Geographic Atrophy in Age-Related Macular Degeneration,” *Am J Ophthalmol*, vol. 237, pp. 58–70, May 2022, doi: 10.1016/j.ajo.2021.11.001.

[20] J. Liu *et al.*, “Diagnosing Persistent Hypertransmission Defects on En Face OCT Imaging of Age-Related Macular Degeneration,” *Ophthalmol Retina*, vol. 6, no. 5, pp. 387–397, May 2022, doi: 10.1016/j.oret.2022.01.011.

[21] S. Copete, I. Flores-Moreno, J. A. Montero, J. S. Duker, and J. M. Ruiz-Moreno, “Direct comparison of spectral-domain and swept-source OCT in the measurement of choroidal thickness in normal eyes,” *British Journal of Ophthalmology*, vol. 98, no. 3, pp. 334–338, Mar. 2014, doi: 10.1136/bjophthalmol-2013-303904.

[22] S. Schmitz-Valckenberg *et al.*, “Interreader Agreement and Longitudinal Progression of Incomplete/Complete Retinal Pigment Epithelium and Outer Retinal Atrophy in Age-Related Macular Degeneration,” *Ophthalmol Retina*, vol. 7, no. 12, pp. 1059–1068, Dec. 2023, doi: 10.1016/j.oret.2023.07.021.

[23] Z. Wu *et al.*, “OCT Signs of Early Atrophy in Age-Related Macular Degeneration: Interreader Agreement: Classification of Atrophy Meetings Report 6,” in *Ophthalmology Retina*, Elsevier Inc., Jan. 2022, pp. 4–14. doi: 10.1016/j.oret.2021.03.008.

[24] S. B. Velaga, M. G. Nittala, A. Hariri, and S. R. Sadda, “Correlation between Fundus Autofluorescence and En Face OCT Measurements of Geographic Atrophy,” *Ophthalmol Retina*, vol. 6, no. 8, pp. 676–683, Aug. 2022, doi: 10.1016/j.oret.2022.03.017.

[25] Y. Shi, J. Yang, W. Feuer, G. Gregori, and P. J. Rosenfeld, “Persistent Hypertransmission Defects on En Face OCT Imaging as a Stand-Alone Precursor for the Future Formation of Geographic Atrophy,” *Ophthalmol Retina*, vol. 5, no. 12, pp. 1214–1225, Dec. 2021, doi: 10.1016/j.oret.2021.02.004.

[26] J. Mai *et al.*, “Comparison of Fundus Autofluorescence Versus Optical Coherence Tomography–based Evaluation of the Therapeutic Response to Pegcetacoplan in Geographic Atrophy,” *Am J Ophthalmol*, vol. 244, pp. 175–182, Dec. 2022, doi: 10.1016/j.ajo.2022.06.023.

[27] U. Schmidt-Erfurth *et al.*, “Disease Activity and Therapeutic Response to Pegcetacoplan for Geographic Atrophy Identified by Deep Learning-Based Analysis of OCT,” *Ophthalmology*, vol. 132, no. 2, pp. 181–193, Feb. 2025, doi: 10.1016/j.ophtha.2024.08.017.

[28] Y. Yang and H. Dunbar, “Clinical Perspectives and Trends: Microperimetry as a Trial Endpoint in Retinal Disease,” *Ophthalmologica*, vol. 244, no. 5, pp. 418–450, 2021, doi: 10.1159/000515148.

[29] K. Birner *et al.*, “Structure-Function Correlation of Deep-Learning Quantified Ellipsoid Zone and Retinal Pigment Epithelium Loss and Microperimetry in Geographic Atrophy,” *Invest Ophthalmol Vis Sci*, vol. 66, no. 3, p. 26, Mar. 2025, doi: 10.1167/iovs.66.3.26.

[30] S. Riedl *et al.*, “The Effect of Pegcetacoplan Treatment on Photoreceptor Maintenance in Geographic Atrophy Monitored by Artificial Intelligence–Based OCT Analysis,” in *Ophthalmology Retina*, Elsevier Inc., Nov. 2022, pp. 1009–1018. doi: 10.1016/j.oret.2022.05.030.

[31] S. B. Velaga, M. G. Nittala, R. K. Konduru, F. Heussen, P. A. Keane, and S. R. Sadda, “Impact of optical coherence tomography scanning density on quantitative analyses in neovascular age-related macular degeneration,” *Eye*, vol. 31, no. 1, pp. 53–61, Jan. 2017, doi: 10.1038/eye.2016.260.

[32] L. Terry *et al.*, “Automated Retinal Layer Segmentation Using Spectral Domain Optical Coherence Tomography: Evaluation of Inter-Session Repeatability and Agreement between Devices,” *PLoS One*, vol. 11, no. 9, p. e0162001, Sep. 2016, doi: 10.1371/journal.pone.0162001.

[33] S. Chandra, R. Rasheed, P. Sen, D. Menon, and S. Sivaprasad, “Inter-rater reliability for diagnosis of geographic atrophy using spectral domain OCT in age-related macular degeneration.,” *Eye (Lond)*, vol. 36, no. 2, pp. 392–397, Feb. 2022, doi: 10.1038/s41433-021-01490-5.

Figure legends

Figure 1. *Examples of spatial overlap between manually annotated hypertransmission and RPE loss within each device for an eye with a unifocal GA lesion showing good spatial overlap* ***(A-F)*** *and for an eye with a multifocal GA lesion demonstrating fair spatial overlap* ***(G-L)****. En face projections are derived from manual OCT B-scan annotations and overlaid on the corresponding nIR acquired simultaneously with the OCT in Spectralis and Cirrus, and overlaid on the corresponding CFP acquired simultaneously with the OCT in Maestro2.* ***D-F)*** *demonstrate a good spatial overlap (purple) between projected 2-D area of hypertransmission (red) based on the A-scan per B-Scan annotations and RPE loss (blue) based on the pixel-wise layer annotations.* ***J-L)*** *demonstrate a fair spatial overlap (purple) between projected 2-D area of hypertransmission (red) based on the A-scan per B-Scan annotations of RPE loss based on the pixel-wise layer annotations. CFP = color fundus photography, Cirrus = Cirrus 5000 HD-OCT (Carl Zeiss Meditec, Inc.), Maestro2 = Topcon 3D OCT Maestro2 (Topcon), nIR = near infrared reflectance, RPE = retinal pigment epithelium, Spectralis = Spectralis HRA + OCT (Heidelberg Engineering).*

Figure 2. *Representative OCT B-scans acquired using the three OCT devices (Spectralis, Maestro2, and Cirrus) displaying qualitative differences in image quality. The Spectralis B-scans (left column) show enhanced layer contrast, reduced speckle noise, and improved delineation of retinal structure. In comparison, the Maestro2 (middle column) and Cirrus (right column) B-scans exhibit lower contrast and increased speckle noise levels.*

Figure 3. *Bland-Altman plots illustrating the bias and variability of RPE loss and HT area measurements in mm^2 across Spectralis, Maestro2 and Cirrus OCT devices. The 95% Limits of Agreement (Mean Difference ±1.96 Standard Deviation of the Difference) are plotted with red. The blue line indicates the Mean Difference between the measurements in mm^2. Cirrus = Cirrus 5000 HD-OCT (Carl Zeiss Meditec, Inc.), HT = hypertransmission, Maestro2 = Topcon 3D OCT Maestro2 (Topcon), RPE = retinal pigment epithelium, Spectralis = Spectralis HRA + OCT (Heidelberg Engineering).*

Figure 4. *Bland-Altman plots illustrating the bias and variability of RPE loss and HT area measurements in √mm^2 across Spectralis, Maestro2 and Cirrus OCT devices. The*

95% Limits of Agreement (Mean Difference ±1.96 Standard Deviation of the Difference) are plotted with red. The blue line indicates the Mean Difference between the measurements in √mm². Cirrus = Cirrus 5000 HD-OCT (Carl Zeiss Meditec, Inc.), HT = hypertransmission, Maestro2 = Topcon 3D OCT Maestro2 (Topcon), RPE = retinal pigment epithelium, Spectralis = Spectralis HRA + OCT (Heidelberg Engineering).

Tables

Table 1. Technical Properties of each OCT device (adapted from [10])

Device	Wavelength	Scanning Speed (A-scan/s)	Axial resolution*
SD-OCT Zeiss Cirrus 5000 HD-OCT	840 nm	27,000/s	5 µm
SD-OCT Heidelberg Spectralis HRA + OCT	870 nm	85,000/s	7 µm
SD-OCT Topcon 3D OCT-1 Maestro2	840 nm	50,000/s	6 µm

*The axial resolution value refers to the tissue-equivalent resolution.

SD = spectral-domain; OCT = optical coherence tomography

Table 2. Descriptive Statistics, Intraclass Correlation Coefficient and Dice similarity coefficient on Area of Hypertransmission and RPE loss across the three OCT devices

	Median (IQR)						ICC [Spectralis - Maestro – Cirrus]	
	Spectralis		Maestro2		Cirrus			
Hypertransmission area [mm²]	1.11	(0.85 to 2.31)	1.18	(0.69 to 1.98)	0.76	(0.53 to 1.72)	0.83	(95% CI 0.74 to 0.90)
RPE loss area [mm²]	0.77	(0.47 to 1.63)	0.61	(0.44 to 1.43)	0.54	(0.31 to 1.18)	0.80	(95% CI 0.69 to 0.88)
DSC (HT-RPE-area Overlap)	0.76	(0.64 to 0.85)	0.72	0.60 to 0.80)	0.73	(0.60 to 0.81)		

CI = Confidence Interval; Cirrus = Cirrus 5000 HD-OCT (Carl Zeiss Meditec, Inc.), DSC = Dice similarity coefficient, HT = Hypertransmission, ICC = intraclass correlation coefficient, Maestro2 = Topcon 3D OCT Maestro2 (Topcon), RPE = retinal pigment epithelium, Spectralis = Spectralis HRA + OCT (Heidelberg Engineering).

Table 3. Mean Difference, Standard Deviation of Difference, Upper and Lower Limits of Agreement from the Bland-Altmann-Plots across all Pairwise OCT device Comparisons

Device Comparison	Hypertransmission area [mm^2]	RPE loss area [mm^2]
	Mean Difference	Mean Difference
Cirrus - Spectralis	-0.43	-0.25
Maestro2 - Spectralis	-0.05	-0.11
Cirrus - Maestro2	-0.39	-0.14
	Standard Deviation of Difference	**Standard Deviation of Difference**
Cirrus - Spectralis	± 1.03	± 0.81
Maestro2 - Spectralis	± 0.31	± 0.36
Cirrus - Maestro2	± 1.00	± 0.76

	Upper LoA	Lower LoA	Upper LoA	Lower LoA
Cirrus - Spectralis	1.58	-2.44	1.34	-1.84
Maestro2 - Spectralis	0.57	-0.66	0.6	-0.82
Cirrus - Maestro2	1.59	-2.36	1.34	-1.62

CI = confidence interval, Cirrus = Cirrus 5000 HD-OCT (Carl Zeiss Meditec, Inc.), HT = Hypertransmission, LoA = Limits of Agreement, Maestro2 = Topcon 3D OCT Maestro2 (Topcon), RPE = retinal pigment epithelium, Spectralis = Spectralis HRA + OCT (Heidelberg Engineering).